Joint Narrowband Interference Detection and Channel Estimation for Wideband OFDM

Niels Hadaschik, Irma Zakia, Gerd Ascheid, Heinrich Meyr
Institute for Integrated Signal Processing Systems, RWTH Aachen University, Templergraben 55, 52056 Aachen, Germany
{hadaschik, zakia, ascheid, meyr}@iss.rwth-aachen.de

***Abstract*— Narrowband interference reduces performance of present transmission systems, and will do so in the future to an even higher extent. The interference mainly hinders a correct data signal detection. But it may already have distorted the channel estimation, even for more carriers than the one, actually containing the carrier of the narrowband interferer. Therefore it is substantial to correctly detect the interferer power and its position in the frequency grid. This paper discusses an interference detection scheme in interaction with a preamble based channel estimation for the MB-OFDM standard. It covers the fact that due to large subcarrier channel power fluctuations, either detection probability is poor because of high thresholds, or reduced thresholds make rise to the false alarm probability.**

I. Introduction

Wideband OFDM transmission has been a widely discussed topic in the past few years, as OFDM is a very flexible and robust transmission technique in terms of coping with multipath fading. But as coexisting narrowband systems operate in the same spectral range narrowband interference (NBI) becomes an important topic. Coexisting systems may be systems operating in the same freely usable spectrum like e.g. Bluetooth in the ISM band or licensed systems in their frequency range, where our system is just tolerated with very low spectral densities. The latter one is the UWB approach, for which the Multiband-OFDM (MB-OFDM) [1] standard is an implementation also applying frequency-hopping.

In any case, this NBI is often characterized by a much higher power concentration in isolated subcarriers than that of the OFDM symbol. This renders the transmitted symbols in at least one subcarrier unusable for reasonable data transmissions. Due to leakage effects because of the limited DFT window length the distortion also significantly leaks into neighboring subcarriers causing additional degradation in terms of the BER or PER even for relatively weak interferers.

In [2] the NBI is combatted with estimation and cancellation techniques in frequency domain and in [3] based on adaptive filtering in time domain. Reference [2] ignores a first acquisition and assumes the center frequency of the interferer known, while [3] needs mute periods where no signal is transmitted for adaptation to the NBI. [4] discusses the topic of NBI with the focus on ADC performance in conjunction with an analogue notch filter and assumes the NBI to be known. The text [5] introduces for a similar scenario a blind NBI detection which operates on a whole burst.

Interference can easily be detected, if sensing the otherwise void channel before transmission, even for relatively low interference power by using simple power detection schemes in frequency domain. However, it is shown here that if the interference detection is supposed to be based on the received preamble or data symbols, power detection of weak interferers in frequency domain is severely harmed by the OFDM symbol and the variations of the channel.

Hence, in this work a multistage approach is proposed, where the NBI detector is combined with a channel estimator, both working on the burst preamble. Therefore in a first step, NBI is pre-detected and, afterwards, the channel is estimated considering the acquired/assumed knowledge of the interference as well as channel covariance information. Since the LMMSE channel estimator comprises smoothing of the channel snapshots in frequency domain, still an acceptable estimate of the channel can be interpolated from neighboring data symbols. Based on this preliminary channel estimate, the channel fluctuations can be subtracted from the received signal leaving – ideally – the additive noise and the interference in the signal. This signal may be fed back into the detector, making it possible to significantly lower the threshold, and thereby, increase the detector sensitivity or lower the probability of false alarm. With these detected interferers, the channel estimate can be re-initiated based on our improved knowledge of the interference situation.

The remaining text is structured as follows: in section II the models of the OFDM signals, the channel and the NBI are introduced. Section III then provides a short motivational analysis of the impact of channel variations on the signal detection. Section IV introduces the joint interference detection and channel estimation, before it shortly explains the employed interference suppression, engaging in the system at the demodulation/soft bit generation. In section V some simulations are discussed and in section VI the work is summarized.

II. Signal and Channel Model

The transmission model simplifies the signal model of MB-OFDM in order to clarify the success of the underlying techniques. Frequency hopping is being switched off like envisioned for some modes of this standard. Additionally, the code rate is being fixed at $r = 1/3$, and no further spreading of the transmitted signal is applied. The employed code is the one foreseen for MB-OFDM [1].

The dimension of the DFT and with it the total number of subcarriers per OFDM symbol is $K = 128$. The channel

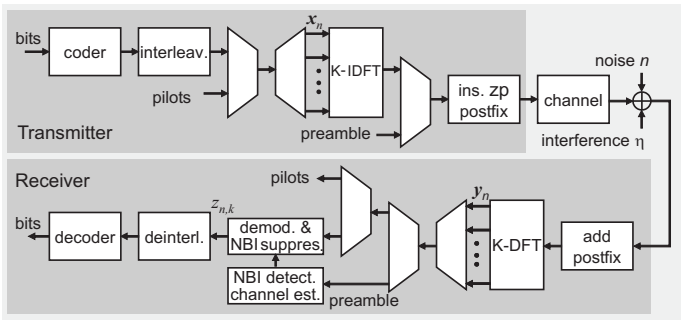

Fig. 1. OFDM System with Interference Detection

estimation will be based on a preamble of two OFDM symbols known to the receiver. The preamble symbols, here, consist of random QPSK symbols on all subcarriers except for the DC carrier and 5 carriers at the edges of the spectrum, which are null carriers. The coded and interleaved data bits are mapped onto a QPSK constellation and are transmitted via the 100 data subchannels. The 12 pilot subcarriers are randomly QPSK modulated and inserted in between at a distance of 10 subcarriers. The additional 10 subcarriers (if the null carriers are also considered for the data symbols), here, contain QPSK data, but are not exploited in this work.

Fig. 1 shows the signal flow in transmitter, channel and receiver in terms of a block diagram. The subcarrier data is transformed to time domain by a K-point DFT and after each K samples of an OFDM symbol N_{Gd} zero samples are appended as zero padded postfix. After transmission via the channel this postfix is then added to the leading N_{Gd} samples of the received OFDM symbol in order to emulate a cyclic convolution with the channel. This is necessary in order to suppress intercarrier interference (ICI) after the FFT in the receiver.

The transmission equation for a single OFDM symbol $\boldsymbol{x}_n$ at the symbol time instance n in the frequency domain then becomes

$$\boldsymbol{y}_n \quad = \quad \mathrm{diag}\{\boldsymbol{x}_n\} \cdot \boldsymbol{h} + \boldsymbol{\xi}_n + \boldsymbol{w}_n. \tag{1}$$

where $\boldsymbol{h}$ is the channel that is assumed to be constant for a burst. $\boldsymbol{\xi}_n$ is the interference and $\boldsymbol{w}_n$ the transformed additive gaussian noise term each in frequency domain. For the transmitted signal the short-cut $\boldsymbol{X}_n = \mathrm{diag}\{\boldsymbol{x}_n\}$ is used. The presumption of unit signal power (QPSK) yields $\boldsymbol{X}_n \boldsymbol{X}_n^H = \boldsymbol{I}$.

The next paragraphs will go into detail with channel and interference.

A. Channel

In order to allow for a prove of concept, the channel in time domain $\boldsymbol{c}$ is modelled as a gaussian channel with an exponentially decaying power delay profile (PDP) of $(\nu+1)$ independent channel taps. However, the authors are well aware that, especially for UWB channels, more sophisticated models are in use e.g. [6]. At least for the channel in frequency domain $\boldsymbol{h} = \mathrm{DFT}_K\{\boldsymbol{c}\}$, additional effects of the reported path clustering are of less importance due to the overlaying of the channel taps $\boldsymbol{c}$ in the frequency domain channel $\boldsymbol{h}$. Employing the channel decay factor Λ, the PDP with $(\nu+1)$ channel taps yields

$$\rho_l = \sigma_h^2 \frac{1-e^{-\Lambda}}{1-e^{-\Lambda(\nu+1)}} \cdot e^{-\Lambda l} \quad \text{for } 0 \leqslant l \leqslant \nu. \tag{2}$$

The discrete length of the channel results in $\nu = \lceil B\tau_{\max} \rceil$, where $\tau_{\max}$ is the continuous duration of the channel impulse response and B is the respective bandwidth. The tap power coefficients ρ_l are assembled in the diagonal PDP matrix $\boldsymbol{\rho} = \mathrm{diag}(\rho_0, \cdots \rho_\nu)$ – in fact, it is diagonal because of the independent channel taps.

For simulation purpose the discrete, time channel impulse response is truncated at $\nu+1 < 3/\Lambda$, such that the last channel tap has in average 5% of the power of the first one, which appears to be sufficient for low SNRs.

B. Interference

In the IEEE Selection Criteria [7] for the 802.15.3a an in-band tone interferer is proposed that consists of a simple unmodulated carrier at frequency Δf_i

$$\eta_m = \sqrt{\sigma_\eta^2} e^{j[2\pi \Delta f_i T m + \phi_0]} \tag{3}$$

with power σ_η^2 and a random phase ϕ_0. Channel variations of the interferer channel are neglected. This is valid for very narrowband transmission with symbol intervals well longer than OFDM symbol length e.g. Bluetooth if compared to MB-OFDM. The NBI power leaks into several subcarriers due to the rectangular shaped, temporally limited DFT window

$$\xi_{n,k} = \sqrt{\sigma_\eta^2/K} \cdot e^{j\phi_n} \sum_{m=0}^{N-1} e^{j2\pi[\Delta f_i T - \frac{k}{K}]m} \tag{4}$$

$$= \sqrt{\frac{\sigma_\eta^2}{K}} e^{j[\pi(\Delta f_i T - \frac{k}{K})(N-1)+\phi_n]} \frac{\sin(\pi[\Delta f_i T - \frac{k}{K}]N)}{\sin(\pi[\Delta f_i T - \frac{k}{K}])} \tag{5}$$

where $N = K + N_{\mathrm{Gd}}$. This leakage is a well known effect as already discussed by Slepian in his introduction of the prolate spheroidal functions [8] or more previous works e.g. [2]. This effect on MB-OFDM differs slightly from OFDM systems with cyclic prefix because of different receiver structures.

The NBI power leaking into subcarrier k equals

$$P_{i,k} = \frac{\sigma_\eta^2}{K} \left| \frac{\sin(\pi[\Delta f_i T - k/K]N)}{\sin(\pi[\Delta f_i T - k/K])} \right|^2, \tag{6}$$

and its maximum magnitude is $\sigma_\eta^2 N^2/K$. Fig. 2 displays the leakage power for three interference carriers $K\Delta f_i T = 0, 0.25$ and 0.5, as only the fractional part is important for the shape of the discrete leakage function. $K\Delta f_i T = 0$ represents an interferer right in the center of a subcarrier, while $K\Delta f_i T = 0.5$ is an interferer in between to subcarriers leading to a maximum spread of power. Additionally for $K\Delta f_i T = 0.5$, the underlying frequency domain sampling of the original function is demonstrated. The results can also be shown by simulation to approximately hold true for NBI bandwidths up to the one of the subcarrier bandwidth.

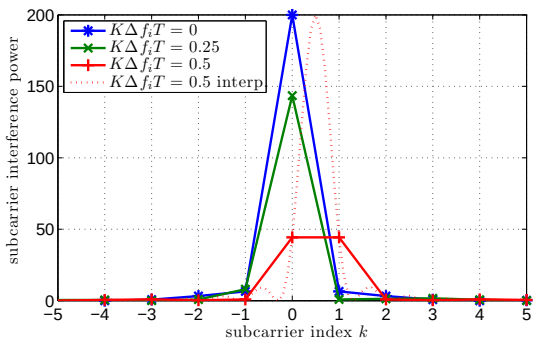

Fig. 2. Interferer leakage power for varying interferer carriers

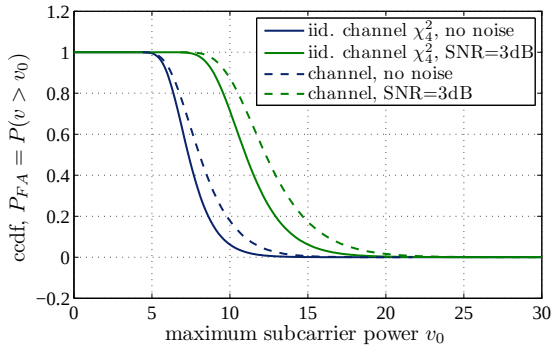

Fig. 3. Probability of the max. subchannel power higher than threshold

III. Motivational Analysis

This section shortly states the problem of detecting a narrowband signal in a fading environment. If the distorted subcarriers are used for conveying training data like in a preamble, it may also increase the mean square error (MSE) of the channel estimation for several subcarriers due to the leakage. This effect additionally spreads out to an even wider range of subcarriers, if the channel estimates are smoothed by lowpass filtering the channel observations.

Hence, reliable interference detection schemes become more and more important, especially, if the power of interference is in the same order of magnitude of the signal plus noise power $|h_k x_k + n_k|^2$. If we assume averaging over both preamble symbols, the decision variable $u_k = \sum_{n=0}^{1} |h_k x_{n,k} + w_{n,k}|^2$ (in fact we skip the division by 2) results. In order to achieve a high detection probability for weak interferers the maximum subcarrier power is compared with a relatively low threshold. But channel fluctuation in subcarrier domain already cause the expected maximum of the subchannel power $v = \max_k\{u_k\}$ in the absence of NBI to be an order of magnitude higher than the average channel gain σ_h^2. This is visible for the complementary cdf (ccdf) $1 - F_v(v)$ of the maximum channel gain in Fig. 3. This is the probability that the maximum channel gain exceeds the value of the abscissa. The two cases depicted represent (a) only the subcarrier channels h_k of power $\sigma_h^2 = 1$ (in black on the left, exponential PDP of 41 samples) and (b) additionally including AWGN at an SNR of 3 dB (on the right). As reference the ccdf for assumed independently, identically χ_4^2-distributed channels are computed and displayed in Fig. 3 for both cases according to

$$P_{\text{FA}}(v) = 1 - F_v(v) \tag{7}$$

$$= 1 - \left[1 - e^{-v/\sigma_f^2} \cdot \left(\frac{v}{\sigma_f^2} + 1\right)\right]^K \tag{8}$$

where the shortcut $\sigma_f^2 = \sigma_h^2 + \sigma_w^2$ is used. However, this approach neglects correlation of the channel in frequency as well as temporal domain explaining the visible inaccuracies.

High outputs of $v = \max_k\{u_k\} > 10$ can be expected already rather often just due to the channel variations and the AWGN as visible in Fig. 3. This causes a high false alarm (FA) [9] probability. Sometimes, channel and noise might even surpass the power of an existing interferer, which causes both a detection miss and a false alarm.

IV. System Components

In the next subsection the adapted system components are introduced which comprise NBI detection, channel estimation and NBI suppression.

A. NBI detection

It is assumed that the receiver possesses no further knowledge on the possible interferer, i.e. the subcarrier comprising the center frequency $\Delta f_i T$ of the NBI as well as the strength of the interferer are unknown to the receiver. Hence firstly, after the DFT the subcarrier with maximum power

$$k_{\text{max}}^{(0)} = \arg\max_k \sum_{n=0}^{1} |y_{n,k}|^2 \tag{9}$$

is found. This power is compared to a threshold to be determined

$$\sum_{n=0}^{1} |y_{n,k_{\text{max}}}|^2 \gtrless \gamma(\sigma_h^2, \sigma_w^2) \tag{10}$$

The threshold depends on channel and noise power but not the NBI carrier $\Delta f_i T$ because it is unknown as well as undetectable due to phase ambiguities. This leads later on to an unavoidable dependency of the detection probability on $\Delta f_i T$. The power of the two successive CE preamble symbols is used for averaging. The respective subcarrier and its surrounding ones ($k_{\text{max}}^{(0)} \pm 1$) are then signalled to the channel estimator together with an estimate of the respective interference power in that subcarrier

$$\widehat{P}_{i,k_i}^{(0)} = \text{pos}\left(\frac{|y_{0,k_i}|^2 + |y_{1,k_i}|^2}{2} - (\widehat{\sigma_h^2} + \widehat{\sigma_w^2})\right) \tag{11}$$

with $k_i \in \{k_{\text{max}}^{(0)}, k_{\text{max}}^{(0)} \pm 1\}$ where $\text{pos}(x) = x$ for $x > 0$ and 0 otherwise. The combined estimate for $\sigma_h^2 + \sigma_w^2$ is attained by averaging over all subcarriers but the $k_i^{(0)}$

$$\widehat{\sigma_h^2} + \widehat{\sigma_w^2} = \frac{1}{2(K-3)} \sum_{k \setminus k_i} (|y_{0,k}|^2 + |y_{1,k}|^2). \tag{12}$$

The previous as well as the following subcarrier of k_{max} are assumed to be harmed by interference, because it is reasonable

to decide in favor of $k_{\max}$ as interferer if $\Delta f_i T$ is in the range $[(\frac{k_{\max}^{(0)}}{K} - \frac{1}{2K}), (\frac{k_{\max}^{(0)}}{K} + \frac{1}{2K})]$. However, for $\Delta f_i T = \frac{k_{\max}^{(0)}}{K} \pm \frac{1}{2K}$, it would be equally sensible to decide in favor of $k_{\max} \pm 1$ respectively, as they contain the same amount of interference power (cf. Fig. 2). As due to phase ambiguity, there is no applicable way of determining the real value of Δf_i, we are on the safer side if we simply assume all k_i as interference and estimate the interference power as in (11).

This simple detection algorithm can be extended to multiple interferers. Therefore, after a first *successful* detection cycle, a second one could be started on the maximum power of the remaining subcarriers all $k \setminus \{k_{\max}^{(0)}, k_{\max}^{(0)} \pm 1\}$ such that this maximum is also compared to the threshold as in (10). This process can then be resumed for further interferers until the threshold is not exceeded any longer or a maximum number of admitted interferers is reached. Then the set of all subcarriers affected by interference $\mathcal{S}^{(0)}$ and their respective interference power $\mathcal{P}^{(0)}$ is signalled to the channel estimator.

A similar proceeding – although not pursued in this work – is possible for "less narrowband" interferers covering several subcarriers even before DFT leakage. The tactic would then be to start at the detected maximum and then proceed comparing in each direction as long as at the next one falls below the threshold. The harmed subcarriers are then gained by extending the measurement range (extension approach). In fact even this detection proposal should be able to detect this "less narrowband" interferers, but the extension approach would save the complexity

B. Channel Estimation

For demonstration, an adapted (with respect to noise and estimated interference) LMMSE channel estimation [10] is used as limit with respect to the achievable MSE performance. The formula for the estimator as derived from theory can, in the interference scenario, be expressed as:

$$\widehat{\boldsymbol{h}}^{(0)} = \boldsymbol{C_{hy}} \boldsymbol{C_{yy}^{-1}} \boldsymbol{y}. \tag{13}$$

The autocorrelation matrix of the received signals $\boldsymbol{y}$ yields

$$\begin{aligned} \boldsymbol{C_{yy}} &= E\{\boldsymbol{y}\boldsymbol{y}^H\} = \boldsymbol{X}\boldsymbol{C_{hh}}\boldsymbol{X}^H + \boldsymbol{C_{\xi\xi}} + \boldsymbol{C_{ww}} && (14) \\ &= \boldsymbol{X}\boldsymbol{C_{hh}}\boldsymbol{X}^H + \boldsymbol{C}_d && (15) \end{aligned}$$

summarizing the effect of noise and interference in the distortion covariance matrix

$$\boldsymbol{C}_d = \boldsymbol{C_{\xi\xi}} + \boldsymbol{C_{ww}} \tag{16}$$

For burst traffic, it is assumed that no temporal channel variation occurs such that the only channel correlations are those in frequency domain characterized by the limited and non-uniform power delay profile of the channel

$$\boldsymbol{C_{hh}} = \boldsymbol{F}_K^{(\nu+1)} \boldsymbol{\rho} \boldsymbol{F}_K^{(\nu+1)^H}. \tag{17}$$

The interference correlation emerges from (6) where the additional non-diagonal samples are neglected for implementation

$$\boldsymbol{C_{\xi\xi}} \approx \mathrm{diag}(P_{i,0}, \cdots P_{i,K}), \tag{18}$$

as they do not have large impact, but they can easily be extracted from $E\{\xi_{k_1}\xi_{k_2}^*\}$. In a real receiver implementation the interference correlation is unknown: for the first place, even the position of the interference must be detected there. As the amount of observations per subcarrier is very limited (in fact it is 2 here), an evaluation of interference cross correlation is of no significance anyway. Thus, the average of the subcarrier powers is extracted from (11) and the estimate of the interference correlation becomes

$$\widehat{C}_{\xi_k\xi_k'}^{(0)} = \begin{cases} \widehat{P}_{i,k}^{(0)} & \text{if } k = k' \text{ and } k \in \mathcal{S}^{(0)} \\ 0 & \text{otherwise.} \end{cases} \tag{19}$$

For the implementation, the preamble symbols are averaged before channel estimation such that

$$\widehat{\boldsymbol{h}}^{(0)} = \boldsymbol{C_{hh}}(\boldsymbol{C_{hh}} + \frac{1}{2} \cdot \boldsymbol{C}_d)^{-1} \cdot \frac{\boldsymbol{X}_0^* \boldsymbol{y}_0 + \boldsymbol{X}_1^* \boldsymbol{y}_1}{2}. \tag{20}$$

results as good approximation of the preamble based LMMSE estimator. Note that therefore the interference (phase) is assumed independent in both preambles and that $\boldsymbol{C_{hh}}$ is hermitian. This channel estimate already provides an estimate for the channel power variation. Thus, in order to remove this variation from the received symbols, it is straight forward to subtract an estimate of the received signal part $\boldsymbol{X}_n\widehat{\boldsymbol{h}}$ from $\boldsymbol{y}_n$ in order to reduce the inherent variance (cf. Fig. 3). The mean square error of the channel estimate σ_ε^2 arises from the diagonal elements of the error covariance matrix

$$\boldsymbol{C}_\varepsilon = \boldsymbol{C_{hh}} - \boldsymbol{C_{hh}}(\boldsymbol{C_{hh}} + \frac{1}{2} \cdot \boldsymbol{C}_d)^{-1} \boldsymbol{C_{hh}}. \tag{21}$$

The authors are well aware that the complexity of the underlying LMMSE channel estimator is far beyond being realizable. The inherent matrix inversion (estimated interference scenario), has a complexity of $\mathcal{O}(K^3)$. The Wiener filter implemented as a vector matrix multiplication itself is of complexity $\mathcal{O}(K^2)$. A promising solution would be an extension of the Wiener filter in temporal domain as e.g. [11] to cope with interference.

C. Joint Iterative Processing

Hence, the remodulated preamble based on the above channel estimates is subtracted from the received signal

$$\boldsymbol{y}_n^{(1)} = \boldsymbol{y}_n - \boldsymbol{X}_n\widehat{\boldsymbol{h}}^{(0)}. \tag{22}$$

which is, with a new set of detected interferers $\mathcal{S}^{(1)}$ and NBI power $\mathcal{P}^{(1)}$, fed back into the NBI detector. There, the maximum

$$k_{\max}^{(1)} = \arg\max_k \sum_{n=0}^{1} |y_{n,k}^{(1)}|^2 \tag{23}$$

is recomputed and the resulting subcarrier powers are once again compared with a threshold $\gamma(\sigma_\varepsilon^2, \sigma_w^2)$, etc. The detector results in new sets $\mathcal{S}^{(1)}$ and $\mathcal{P}^{(1)}$ of NBI positions and NBI power estimates respectively. Together with the original preamble data $\boldsymbol{y}_n$ (n=0,1), they are used for the channel estimation like depicted in Fig. 4. Although further iterations might still improve the detection and estimation results the

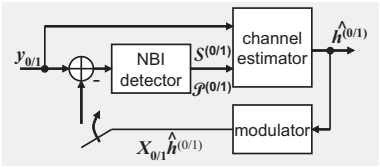

Fig. 4. NBI detector/channel estimator proposal

scheme is skipped here after the second run. Simulations only showed minor gains for further detection/estimation cycles.

The variance of the input to the second detector yields

$$E\{|y_{n,k}^{(1)}|^2\}=E\{|(h_{n,k}-\widehat{h}_{n,k}^{(0)})x_{n,k}+\xi_{n,k}+w_{n,k}|^2\} \quad (24)$$

$$=\sigma_\varepsilon^2+P_{i,k}^{(0)}+\sigma_w^2-2E\{\mathrm{Re}\{\widehat{h}_{n,k}^{(0)}(\xi_{n,k}^*+w_{n,k}^*)\}\}$$

$$\approx\sigma_\varepsilon^2+P_{i,k}^{(0)}+\sigma_w^2-q_{kk}(P_{i,k}^{(0)}+\sigma_w^2) \quad (25)$$

if $q_{m,k}$ is the Wiener filter matrix from (20) the inherent reduction of the interference power by the factor $(1-q_{kk})$ is, in the case of a previously detected interference, marginal because then $q_{kk} \ll 1$. With the variance of $y_{n,k}^{(1)}$ also the variance of the test statistic is reduced.

To assess the estimation performance, a system was simulated at an SNR = 3 dB and and an SIR = 13.25 dB which seems rather high but translates to a subcarrier $\mathrm{SIR}_{\mathrm{sc}} = -9.72$ dB on the mainly afflicted subcarrier, if full alignment of the interferer with the a subcarrier $(K\Delta f_i T = k, k = -K/2, \ldots K/2-1)$ is assumed. This is sufficient to reduce BER performance significantly. In Fig. 5 the channel estimation MSE is displayed for the first (solid line) and the second iteration (dashed) of the detection estimation cycle vs. the threshold of the detector. The above case of perfect alignment $(K\Delta f_i T = k, k = -K/2, -K/2+1, \ldots K/2-1)$ is plotted with 'x'-markers. With '+' the case where $K\Delta f_i T = k + 0.25$ is marked. In both cases, it is is well visible that in the second cycle, a significantly reduced MSE can be achieved up to a threshold of 10 or 12 whereas for thresholds larger than 18 the first detector seems to work better. This is for the reduced power of the subcarrier due to the subtraction of the signal component $\boldsymbol{X}_n\boldsymbol{h}$. Hence, the threshold can be reduced in the second iteration anyway.

Additionally demonstrated in Fig. 5 is the estimation performance when no interference is present (circle marker), i.e. false alarms might occur if the threshold is chosen too low. False alarms mean that valid observations are neglected for estimation, which becomes true for $\gamma < 12$ in the second run and $\gamma < 22$ in the first run. It is obvious that in the second iteration a better performance trade off can be achieved for the MSE (with and without NBI) e.g. with $\gamma = 12$.

These thresholds are chosen because the performance of the system should not degrade in the absence of NBI compared to the case of no NBI detector.

D. NBI Supression

The estimates of the interference power as detected above and already used for channel estimation purpose, are reused for weighing the received data symbols and with them the soft bits of the receive data. Like discussed in [5] the soft symbols are extracted from

$$z_{n,k} = \begin{cases} \frac{\hat{h}_k^{(1)*}\cdot y_{n,k}}{\sigma_w^2+\widehat{P}_{i,k}^{(1)}} & \text{for } k \in \mathcal{S}^{(1)} \\ \frac{\hat{h}_k^{(1)*}\cdot y_{n,k}}{\sigma_w^2} & \text{otherwise} \end{cases} \quad (26)$$

weighting each received data symbol according to its estimated SINR $\frac{\hat{h}_k^*\hat{h}_k}{\sigma_w^2+\widehat{P}_{i,k}^{(1)}}$.

V. Simulation Results

Simulations are performed for an MB-OFDM like system without frequency hopping but – in contrast to the non-frequency hopping modes of MB-OFDM – still with only 2 preamble symbols. The bandwidth of the system is $B = 528$ MHz. The OFDM symbol consists of the $K = 128$ samples IFFT output, $N_{\mathrm{Gd}} = 32$ samples of the zero padded prefix such that that the total signal length $N = 160$. The channel decay constant is chosen as $\Lambda = 1/(25\,\mathrm{ns})$ i.e. the channel length is $\tau_{\max} = 75$ ns, which is approximately equivalent to CM4 of the IEEE 802.15.3a channel models [6] and results in the channel length $\nu + 1 = 41$. If the simple one stage NBI detection algorithm from paragraph IV-A is used, the following channel estimation is based on this detected interference as described in IV-B.

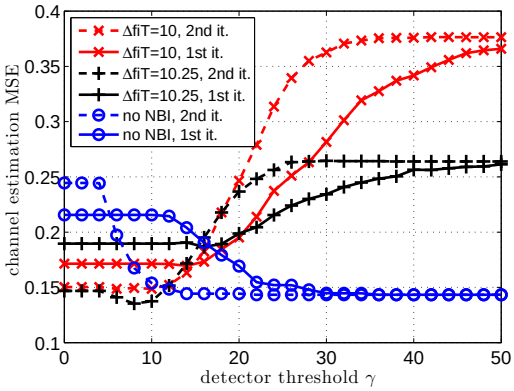

Fig. 5. Channel estimation MSE of both iterations for SNR = 3 dB

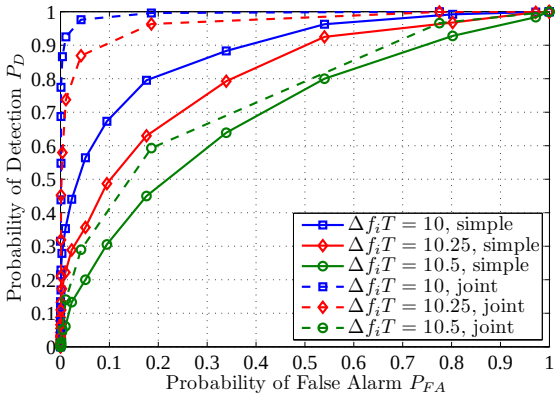

Fig. 6. ROC for NBI detection at SNR = 8 dB and SIR = 13.25 dB

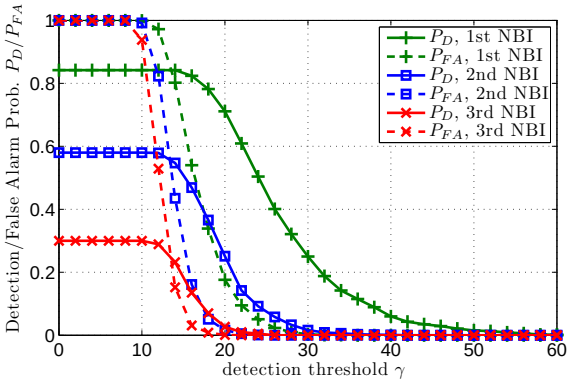

Fig. 7. P_D and P_{FA} with simple detection and 3 interferers

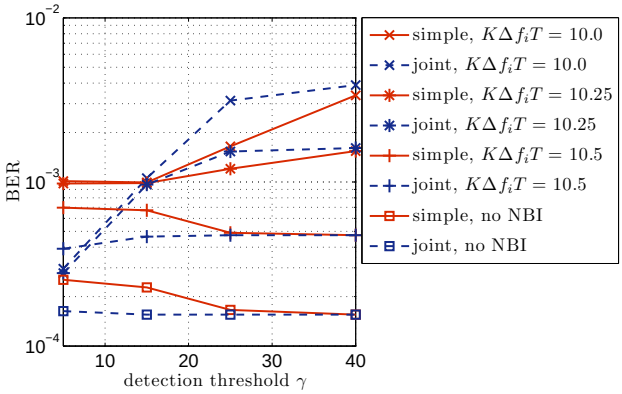

Fig. 9. Single NB Interferer at SIR=13.25 dB and SNR=3 dB

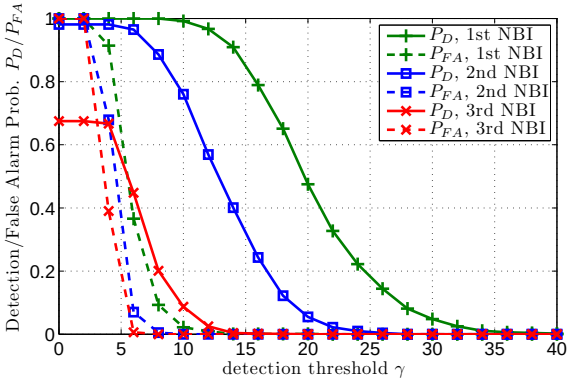

Fig. 8. P_D and P_{FA} with the joint algorithm and 3 interferers

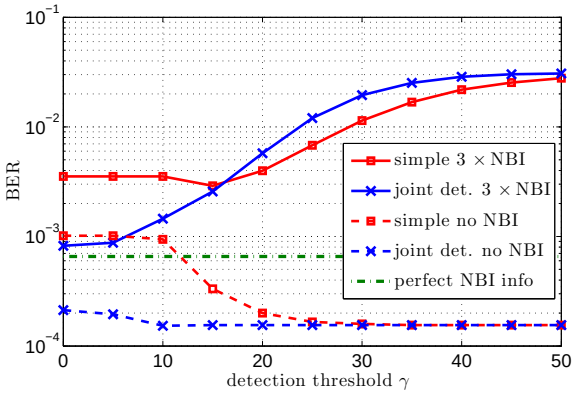

Fig. 10. Three NB interferers at combined SIR=6.5 dB and SNR=3 dB

At first, simulation results concerning a single narrowband interferer are demonstrated. Therefore, since the focus is on signal detection, a ratio of $P_{i,k_{\max}}/(\sigma_h^2+\sigma_w^2) \mathrel{\widehat{=}} 8\,\text{dB}$ at an SNR $= 3\,\text{dB}$ is assumed for the visualization. This corresponds to a subcarrier $\text{SIR}_{\text{sc}} = -9.72\,\text{dB}$ and to the OFDM symbol SIR $= 13.25\,\text{dB}$. It can be shown that even NBI of this strength still rises significantly the BER of MB-OFDM at high rates ($\geqslant 200\,$MBit/s) even with frequency hopping and perfect channel knowledge.

The ROC diagram in Fig. 6 displays the detection probability versus the probability of false alarm for varying NBI carriers $\Delta f_i T$. The characteristics of the simple power detector from section IV-A are plotted as solid lines and those of the joint approach as dashed lines. Since only the fractional part of $K\Delta f_i T$ determines the shape and, with it, the maximum of the interference (cf. Fig. 2), it seems sufficient to base the diagram on 3 distinct NBI carriers with $K\Delta f_i T = 10.0, 10.25$ and 10.5 in order to approximately cover the complete range of interference carriers for detection. 100 channel realizations have been generated and for each 100 detections have been performed.

Obviously, the interference detection performance is best for the aligned interferer $K\Delta f_i T = 10.0$ as then the maximum of the interference function $N^2/K\sigma_\eta^2$ is reached on subcarrier 10. In contrast, the NBI power reaches only 22% of that power at $K\Delta f_i T = 10.5$ rendering a successful detection much more uncertain despite the two chances for correct detection. A remarkable improvement is well visible for the joint scheme and all NBI carriers: the curves approach the point $(P_{FA}=0, P_D=1)$ if compared to the simple detector.

In Fig. 7 and Fig. 8 detection and false alarm probability are depicted vs. the threshold. Therefore, three NBI carriers are chosen coexistent, arbitrary but fixed at $K\Delta f_{i_1} T = -30.25$, at $K\Delta f_{i_2} T = 10.5$ and at $K\Delta f_{i_3} T = 50$. The detection (solid lines) and the false alarm probability (dashed) for each detection cycle are presented. Note that the order of the detections does not tell, which interferer is picked first, second, etc.

Fig. 7 shows the simulated detection and false alarm probabilities for the simple power detector. The most remarkable point is that for thresholds $\gamma < 16$ the detection probabilities reach their maximum, which is not $P_D = 1$, but much lower especially for the third detection, as very often the channel plus noise becomes stronger than all the interferers. Hence, a detection miss and a false alarm occurs. The visible detection miss can be circumvented when more detection trials than interferers are used.

It is obvious that for none of the interferers a sensible trade-off between low false alarm probability and high detection probability can be found. However, employing the joint scheme in Fig. 8 things change significantly: for the first two detections a threshold of $\gamma \approx 10$ seems a good choice. Furthermore, the subtraction of the estimated channel variation becomes beneficial in terms of the reduced probability, that one of the first two detections is erroneous.

In the following, the BER in the presence of NBI is discussed for both detection methods. Therefore, 100 channel realizations are used and for each 100 data packets of 400 bytes data are simulated. The amount of user data corresponds to 48 OFDM symbols after coding and QPSK mapping, 50 symbols together with the preamble. This results in a burst duration of $15.2\,\mu$s, which is more than one order of magnitude smaller than e.g. the minimum frequency hopping interval of Bluetooth.

In Fig. 9 and Fig. 10 display the BER vs. the detection threshold at an SNR = 3 dB. From the very right points in the diagram related to very high detection thresholds γ, it is possible to read the BER if no interference detection would have happened. Especially the case of absent NBI serves as the ultimate lower bound of the BER for this SNR, because it is clearly optimum not to try to (falsely) detect interference, if none is present. Any intervention can only do harm.

For the case of a single interferer in Fig. 9 at an SIR = 13.25 dB, a performance gain can be achieved for all three different interference carriers and the joint scheme (solid lines) and very low detection thresholds. Additionally, the BER remains mostly unharmed from false alarms for absent NBI. For interferers in between two subcarriers e.g. $K\Delta f_i T = 10.5$ almost no gain is achievable, as they cannot be detected properly anyway. That is also the reason that the joint scheme achieves a lower BER for the other NBI carriers at low detection thresholds. The simple detection displayed as solid lines suffers from substantially higher minimum BERs than the joint scheme in all scenarios.

Fig. 10 is now concerned with three interferers present at the time with a combined SIR = 6.5 dB. The power of a single interferer is increased here in order to improve the detection performance in this more severe scenario. The NBI center frequencies are picked as above for the detection and false alarm probabilities. The solid lines indicate the BER for the interference case while the dashed ones deal with the problem of false alarms (no NBI present). Note the maximum of five interference detection cycles (for five detectable interferers): this is especially important for understanding the results at the detection threshold $\gamma = 0$. This means that automatically the five subcarriers with the highest power values are identified by the detector as containing interference. This proceeding achieves amazingly good performance with only small losses in absence of interference for the joint detection and channel estimation. However, looking for a good compromise means here: on the one hand, not to increase the BER for absent NBI, but on the other hand, to gain as much as possible for the case of interference. $\gamma = 10$ for the joint detector and $\gamma = 30$ for the simple one stage detector seem to be good choices. However the BER for the proposed thresholds γ and present NBI is almost 8 times higher for the simple detector than for the joint scheme. This stresses the value of a more intelligent while also much more complex processing. As no phase information on the interference is used the introduced scheme can also be employed if the interference is realized as modulated carrier.

VI. Summary

The presented joint interference detection and channel estimation demonstrates via simulations that it can significantly improve the receiver performance in terms of the BER for high SIR (> 10 dB), if compared to the simple single stage detection algorithm. The gains in the BER together with respective detection thresholds are foreshadowed by the MSE performance of the channel estimator, which, once again, underlines the importance of the channel estimation on the system performance.

For higher code rates, even higher gains are expected due to less code redundancy and, hence, a weaker capability of error correction. Even for an MB-OFDM system including frequency hopping losses of more than 1 dB in the SNR are measured for the 200 MBit/s mode and an SIR = 11.25 dB if no interference is detected, although the NBI just corrupts one third of the OFDM symbols. Furthermore, weaker interferers are much more probable than strong ones, since the related area increases with the radius and the corresponding signal strength decreases with this radius.

As the used LMMSE channel estimator is rather complex, it is beneficial to search for simplified algorithms, that are capable of both, exploiting the channel covariance and realizing an interference suppression in the estimator. A derivation of the joint algorithm from ML or MAP theory and their iterative approximations is a helpful extension, as well as the study of the convergence based on these approximations.

References

[1] Multiband OFDM Alliance, "MBOA PHY Layer Technical Specification V1.1," Published on www.mboa.org, June 2005.

[2] R. Nilsson, F. Sjöberg and J. LeBlanc, "A rank reduced LMMSE canceller for narrowband interference suppression in OFDM-based Systems," *IEEE Transactions on Communications*, vol. 51, no. 12, pp. 2126–2140, Dec. 2003.

[3] A. Coulson, "Narrowband interference in pilot symbol assisted OFDM systems," *IEEE Transactions on Wireless Communications*, vol. 3, no. 6, pp. 2277–2287, Nov. 2004.

[4] K. Shi, Y. Zhou, B. Kelleci, T. Fischer, E. Serpedin, and A. Karsilayan, "Impacts of narrowband interference on OFDM-UWB Receivers: Analysis and Mitigation," *IEEE Transactions on Signal Processing*, vol. 55, no. 3, pp. 1118–1128, March 2007.

[5] S. Vogeler, L. Broetje, K. Kammeyer, R. Rueckriem and S. Fechtel, "Blind Buetooth interference detection and suppression for OFDM transmission in the ISM band," *Conference Record of the Thirty-Seventh Asilomar Conference on Signals, Systems and Computers, 2003*, pp. 703–706, Nov. 2003.

[6] IEEE P802.15 Working group TG3a, "Channel Modelling Sub-Committee Report Final," Published on www.802wirelessworld.com, Feb. 2003.

[7] J. Ellis, K. Siwiak, and R. Roberts, "802.15.3a alt PHY selection criteria," IEEE P802.15 Working group TG3a, Published on www.802wirelessworld.com, Dec. 2002.

[8] D. Slepian, "Prolate Spheroidal Wave Functions, Fourier analysis, and uncertainty, V: the discrete case," *Bell Labs System Technical Journal*, vol. 57, no. 5, pp. 1374–1430, May-June 1978.

[9] S. Kay, *Statistical Signal Processing, Volume II, Detection Theory*, Prentice Hall, Upper Saddle River, NJ, USA, 1st edition, 1998.

[10] H. Meyr, M. Moeneclaey, S. Fechtel, *Digital Communication Receivers: Synchronization, Channel Estimation and Signal Processing*, John Wiley & Sons, New York, NY, 1st edition, 1998.

[11] N. Hadaschik, G. Ascheid, and H. Meyr, "Achievable Data Rate of Wideband OFDM with Data-Aided Channel Estimation," *Proceedings of the IEEE Symposium on Personal Indoor and Mobile Communications (PIMRC) 2006*, Helsinki, Finland, Sep. 2006.